Journal of Geoscience and Environment Protection, 2026, 14(2), 198-222
https://www.scirp.org/journal/gep
ISSN Online: 2327-4344
ISSN Print: 2327-4336

Changes in ENSO Impacts on Ethiopia JJAS Precipitation in Recent Decades

Addisu Belachew Dugo[1,2], Chaoxia Yuan[1*], Asaminew Teshome[2], Mulualem Abera Waza[1,2]

[1]School of Atmospheric Science, Nanjing University of Information Science and Technology (NUIST), Nanjing, China
[2]Ethiopia Meteorology Institute (EMI), Addis Ababa, Ethiopia
Email: *chaoxia.yuan@nuist.edu.cn

How to cite this paper: Dugo, A. B., Yuan, C. X., Teshome, A., & Waza, M. A. (2026). Changes in ENSO Impacts on Ethiopia JJAS Precipitation in Recent Decades. *Journal of Geoscience and Environment Protection, 14,* 198-222.
https://doi.org/10.4236/gep.2026.142011

Received: January 20, 2026
Accepted: February 11, 2026
Published: February 14, 2026

Abstract

Ethiopia's June-September (JJAS) rainfall is crucial for water resources, agriculture, and livelihoods, and exhibits pronounced interannual variability driven by extremely large-scale ocean-atmosphere interactions. The El Niño-Southern Oscillation (ENSO) has long been recognized as the primary source of this variability, exerting strong control on the strength and spatial distribution of Ethiopia's summer rainfall. Using CHIRPS rainfall, ERA5 reanalysis fields, and ENSO and AMO climate indices, we employ correlation, regression, composite, and sliding-window analyses, complemented by moisture flux and circulation diagnostics. Results show a decline in the ENSO-JJAS rainfall correlation, weakening from r = −0.71 to r = −0.59, with strong relationships over central and northern Ethiopia becoming weak or statistically insignificant after 2001. AMO, on the other hand, has become more influential, with correlations increasing from r = 0.094 to r = 0.556. Atmospheric diagnostics indicate reduced ENSO-related circulation anomalies and moisture convergence over Ethiopia, alongside enhanced contributions to monsoon moisture transport from the Atlantic sector. These findings suggest a shift away from ENSO-dominated control toward a broader multi-basin influence, in which ENSO alone is no longer sufficient to explain JJAS rainfall variability. Therefore, seasonal forecasting systems for Ethiopia should incorporate Atlantic climate variability in addition to ENSO to improve predictive skill.

Keywords

ENSO, Ethiopia, JJAS Rainfall, Decadal Shift, Teleconnection, Variability

1. Introduction

In Ethiopia, rainfall is an important meteorological variable. Approximately 85% of the population is involved in rain-fed agriculture and is therefore vulnerable to

anomalously high or low rainfall amounts in the crop-growing season. Over 80% of the country's crop production depends on JJAS rainfall, directly connecting to agricultural results, water resources, and food security (Tafere et al., 2013). Rainfall over Ethiopia indicates large variations across time and space, and extreme variations have historically been associated with severe drought and floods, leading to significant socio-economic impacts (Seleshi & Zanke, 2004). The complex temporal and spatial variability is driven by sea surface temperature anomalies in the Pacific and Atlantic Oceans (Degefu et al., 2017). JJAS rainfall variability further shows remarkable shifts in magnitude, spatial distribution, and predictability over recent decades (Endris et al., 2019).

The El Niño Southern Oscillation (ENSO) drives the largest fraction of Earth's year-to-year climate systems (Vialard et al., 2025). ENSO influences the Ethiopian climate through large-scale atmospheric circulation, moisture transport, and vertical motion. Earlier studies have demonstrated that ENSO significantly governs Ethiopian JJAS rainfall, with El Niño events related to suppressed rainfall, and La Niña events tending to increase precipitation over summer rainfall, benefiting regions (Nicholson, 2017), making ENSO an essential seasonal climate forecast. ENSO JJAS correlation is weakening, perhaps due to increased interactions with other oceanic basins, altered Walker circulation, and background climate change (Endris et al., 2019). This study demonstrates the statistical significance of reassessing how ENSO and other climatic factors influence the variability of rainfall in Ethiopia.

Ethiopian JJAS rainfall is influenced by ENSO, as well as other large-scale ocean-atmosphere modes, especially the Atlantic Multidecadal Oscillation (AMO). Through atmospheric teleconnections, AMO indirectly modulates Ethiopian rainfall by altering hemispheric sea surface temperature gradients and large-scale circulation (Zhang & Delworth, 2006; Monerie et al., 2019); (Kucharski et al., n.d.). Previous studies indicate that variability in Atlantic conditions can either amplify or counteract ENSO-related impacts on Ethiopian rainfall variability (Endris et al., 2019; Nicholson, 2017). These multi-basin influences contribute to the evolving nature of rainfall patterns across Ethiopia.

Notably, understanding of individual climate drivers is a critical knowledge gap regarding the combined and evolving impacts of ENSO and Atlantic variability on Ethiopia's JJAS rainfall in recent decades. Most previous studies have focused on single climate modes, with limited attention to the temporal evolution of teleconnections under a warming climate. The relative strengthening of AMO effects simultaneously with a weakening ENSO signal emphasizes the need for a combined assessment to improve seasonal forecasting, early warning systems, and climate-resilient agriculture and water management.

The objective of this study is to assess changes in the influences of ENSO on Ethiopia's JJAS rainfall in recent decades and to examine how the background Atlantic climate variability, especially the Atlantic Multidecadal Oscillation (AMO), is associated with these changes. Understanding these interactions is essential, as

shifts in large-scale ocean-atmosphere modes can alter teleconnection pathways, modify regional circulation, and reshape seasonal rainfall predictability. The study integrates high-quality recorded rainfall datasets with ENSO and AMO indices and applies time-varying and spatial analysis to characterize evolving teleconnections and their implications for climate risk management in Ethiopia.

The remainder of the paper is organized as follows: Section 2 describes the Data and Methods, and Section 3 describes Results and Discussions. Section 4 presents the summary and conclusion.

2. Data and Methods

2.1. Study Area

Ethiopia is located in the Horn of Africa between 3˚N and 15˚N latitude and 33˚E to 48˚E longitude (**Figure 1**). Its geography is quite varied, ranging from highlands that are more than 4600 m above sea level to the Danakil Depression around −126 m (Negash & Waza, 2025). Although the climate is primarily tropical, elevation and large-scale atmospheric circulation patterns have a significant impact on its regional and temporal variability (Segele & Lamb, 2005). Most of Ethiopia's annual rainfall occurs during the main rainy season, known locally as kiremt, which spans June to September (JJAS) and provides 50% - 80% of annual precipitation, particularly over the central, western, northern, and highlands (Korecha & Barnston, 2007; Diro et al., 2011). The seasonal rainfall distribution is strongly controlled by topography and large-scale ocean-atmosphere teleconnections, such as El Niño-Southern Oscillation (ENSO) and other climatic indices. **Figure 1**

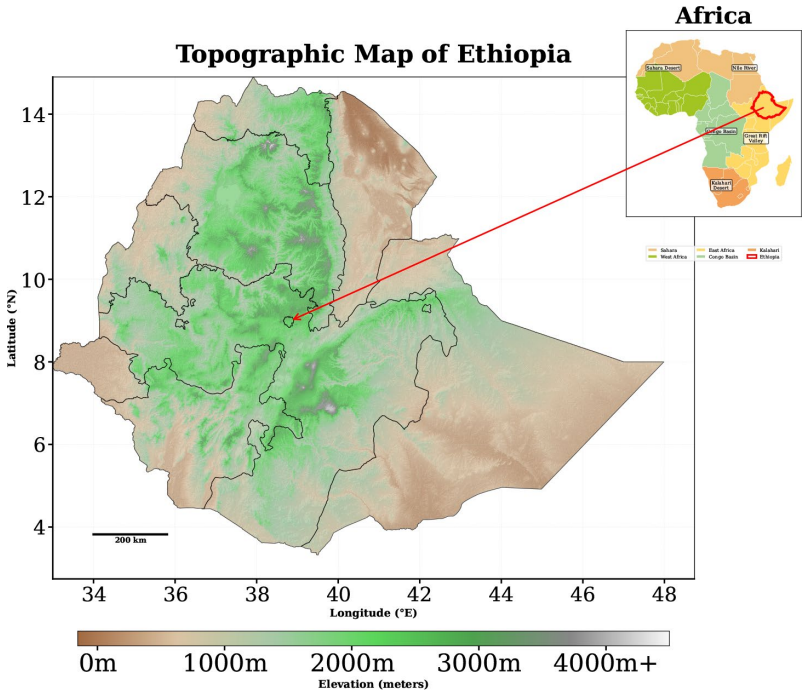

Figure 1. Topographic map of Ethiopia showing elevation (meters) and major geographic features.

presents a high-resolution topographic map of Ethiopia, generated using SRTM elevation data (http://srtm.csi.cgiar.org/wp-content/uploads/file/srtm_5x5/TIFF/) and the natural Earth country boundaries (http://www.naturalearthdata.com/), with an inset highlighting the country's location with Africa.

2.2. Data and Methodology

2.2.1. Data

1) CHIRPS Data

This study applies observational and reanalysis datasets to examine changes in ENSO affecting Ethiopia's JJAS rainfall. Monthly precipitation is obtained from the Climate Hazards Group Infrared Precipitation with Station data (CHIRPS) v2.0, high-resolution (0.05˚ × 0.05˚) datasets covering 1981-2023 (Diro et al., 2011; Funk et al., 2015). CHIRPS widely represents Ethiopia's rainfall variability and teleconnection and is widely used in hydro and climate studies (Taye et al., 2021; Korecha & Sorteberg, 2013; Manatsa et al., 2008; Korecha & Barnston, 2007). The CHIRPS V2.0 monthly dataset is available at: https://data.chc.ucsb.edu/products/CHIRPS–2.0/global_monthly/netcdf/chirps-v2.0.monthly.nc

2) Climatic Indices Data

The Niño 3.4 index provided by the NOAA Climate Prediction Center, defined as sea surface temperature (SST) anomalies averaged over (5˚N-5˚S, 170˚-120˚W) (Tang et al., 2025), is a key indicator for ENSO variability linked to Ethiopian rainfall (Yang et al., 2025; Bayr et al., 2025; Korecha & Barnston, 2007). In addition to ENSO, the Atlantic Multidecadal Oscillation (AMO) indices were included (Camberlin, 2023). The Niño 3.4 and AMO datasets are available from (https://psl.noaa.gov/data/timeseries/month/Nino34/), and (https://psl.noaa.gov/data/timeseries/AMO/), respectively.

3) Reanalysis Data

Large-scale dynamical mechanisms related to ENSO teleconnections were examined using ERA5 reanalysis data from the European Center for Medium Range Weather Forecasts (ECMWF). Variables consist of zonal (u) and meridional (v) winds, specific humidity, vertical velocity (omega), and geopotential height at multiple pressure levels. ERA5 provides global fields at 0.25˚ × 0.25˚ resolution and represents circulation features relevant to Ethiopian monsoon systems (Bell et al., 2021; Zhang et al., 2021; Chen et al., 2022; Waza et al., 2025). Those datasets were obtained from: (https://cds.climate.copernicus.eu/datasets/reanalysis-era5-single-levels-monthly-means?tab=download).

2.2.2. Methodology

To assess long-term variations in the ENSO-rainfall relationship, the study period was split into an early period (1981-2001) and a current era (2002-2023). To objectively justify this division, we applied a Monte Carlo Pettitt non-parametric change-point detection test to the 10-year running ENSO-rainfall correlation. Statistically significant regime shift is tested and identified in the 2001/2002 transi-

tion (p = 0.0001), supporting the two-period separation used through the analysis.

Sliding window correlation was then applied to diagnose changes in teleconnection strength and spatial structure between the two periods. During the study, monthly data were aggregated into JJAS seasonal totals, and rainfall anomalies were calculated relative to the 1991-2020 climatological baselines to isolate interannual variations (Arguez et al., 2012). A collection of statistical methods was applied to evaluate teleconnection strength and diagnose its temporal evolution.

1) Standardized Rainfall and Atmospheric Anomalies

Standardized rainfall anomalies and atmospheric anomalies were calculated as:

$$Std.A = \frac{X - \bar{X}}{\sigma} \tag{1}$$

where X is the observed seasonal value, $\bar{X}$ is the climatological mean, and σ is the standard deviation.

2) Pearson correlation and regression

To quantify teleconnection strength, Pearson correlation analysis was implemented between JJAS rainfall anomalies and climate indices. The linear relationship between two variables is measured by the Pearson correlation and ranges from −1 to +1, indicating perfect negative and positive correlations. The Pearson correlation coefficient formula is defined as:

$$r = \frac{\sum(x_i - \bar{x})(y_i - \bar{y})}{\sqrt{\sum(x_i - \bar{x})^2 (y_i - \bar{y})^2}} \tag{2}$$

where x_i, y_i is the actual value at time *i*, and $\bar{x}, \bar{y}$ are the mean values.

Linear regression analysis was used to determine the sensitivity of JJAS rainfall anomalies to climate indices variability. Regression slopes represent the magnitude of rainfall change per unit Niño 3.4 anomaly, while the coefficient of determination (R^2) was used to estimate the fraction of rainfall variance explained by ENSO.

$$Y = \beta_0 + \beta_1 X + \epsilon \tag{3}$$

$$R^2 = 1 - \frac{\sum\left(Y - \hat{Y}\right)^2}{\sum\left(Y - \bar{Y}\right)^2} \tag{4}$$

3) Composite Analysis

Composite analysis was implemented for El Niño, La Niña, and neutral phases to examine the characteristics of rainfall, circulation, and moisture anomaly patterns. Composite anomalies were calculated as the difference between the mean of ENSO event years and the long-term climatological mean.

4) Man-Kendal Trend

Long-term trends in rainfall and ENSO indices were evaluated using the nonparametric Mann-Kendall test, with trend magnitude quantified by the Sen's slope estimator. Its formula is defined as

$$S = \sum_{i=1}^{n-1} \sum_{j=i+1}^{n} \text{sign}\left(x_j - x_i\right) \tag{5}$$

where the sign function is used to evaluate whether x_j is greater than, equal to, or less than x_i. x_j And x_i are the sequential data values, n is the length of the dataset, and

$$\operatorname{sign}\left(x_j - x_i\right) = \begin{cases} 1 & \text{if } \left(x_j - x_i\right) > 0 \\ 0 & \text{if } \left(x_j - x_i\right) = 0 \\ -1 & \text{if } \left(x_j - x_i\right) < 0 \end{cases} \tag{6}$$

where x_i, x_j are sequential values in the time series.

The test statistic Z is then calculated as follows

$$Z = \begin{cases} \dfrac{S-1}{\sqrt{\operatorname{var}(S)}} & \text{if } S > 0 \\ 0 & \text{if } S = 0 \\ \dfrac{S+1}{\sqrt{\operatorname{var}(S)}} & \text{if } S < 0 \end{cases} \tag{7}$$

where $\operatorname{var}(S)$ is the variance of the Mann-Kendall S statistic, which is computed considering ties in the data present. The value of Z is then used to determine the significance of the trend. A two-tailed Student's t-test with a 95% confidence level was used to assess statistical significance.

5) K-means Clustering

To identify homogeneous regions, K-means clustering was applied based on the ENSO-rainfall correlations. Grid-point correlation coefficients between the ENSO index, computed across the common analysis period, and the JJAS seasonal mean rainfall generated from CHIRPS data served as the input variable for the clustering analysis. The clustering was performed exclusively for grid cells located within the Ethiopian boundary, as defined by the national shapefile. Before analyses, missing values were excluded, and four clusters ($k = 4$) were specified to delineate regions exhibiting similar ENSO-driven rainfall response characteristics (Zhang & Fan, 2026).

3. Results and discussion

3.1. JJAS Rainfall, Moisture Flux Divergence, and Transport Climatology

Figure 2 presents the JJAS climatology of seasonal rainfall, vertically integrated moisture transport at 850 hPa, and moisture-flux divergence across Ethiopia from 1981-2023. The seasonal totals of rainfall over the northwestern and central Ethiopian Highlands exceed 1400 mm, closely reflecting the influence of complex topography and strong orographic lifting. On the other hand, markedly lower rainfall over eastern Ethiopia and the Horn arises from steep topographic gradients and associated rain-shadow effects. The low-level circulation is characterized by persistent southwesterly to westerly winds, accompanied by moisture flux magnitudes of approximately 40 - 80 $kg \cdot m^{-1} \cdot s^{-1}$, with locally enhanced values over western Ethiopia. Moisture transport reveals a coherent multi-branch monsoon

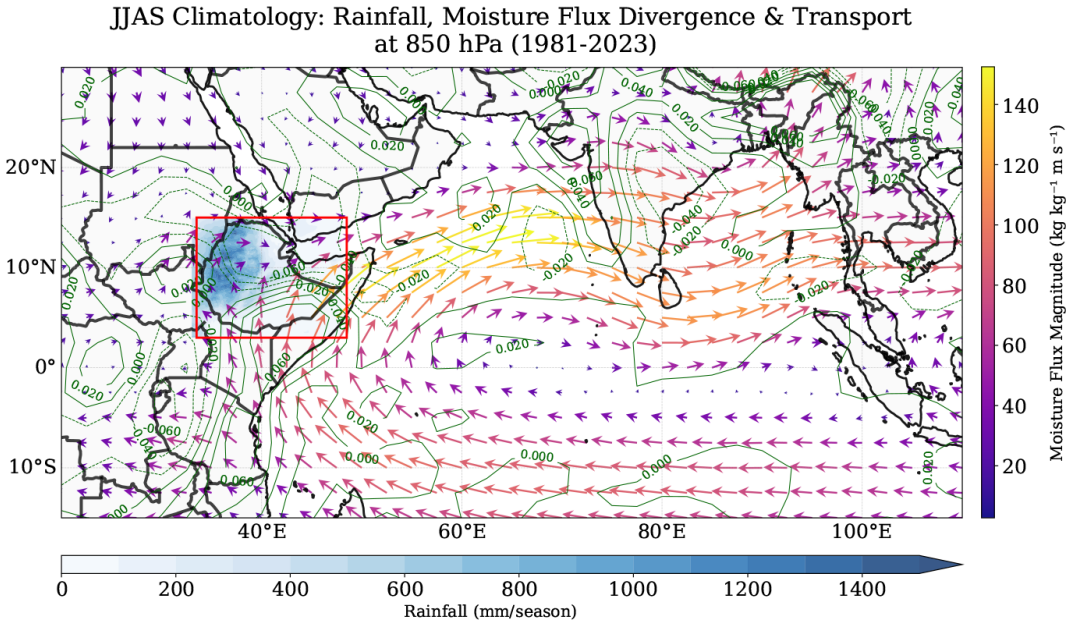

Figure 2. JJAS climatology of rainfall, moisture-flux divergence, and 850 hPa moisture transport over Ethiopia (1981-2023).

inflow, dominated by strong westerly fluxes from the Congo Basin and southwesterly inflow linked to the cross-equatorial Somali Jet, converging over the highlands. The Ethiopian Highlands cause the low-level winds to decrease and shift direction, which causes moisture to build up and converge over the highlands. This demonstrates the crucial role that orographic lifting and monsoon-driven moisture influx play in regulating the intensity and spatial distribution of Ethiopia's JJAS rainfall.

3.2. Interannual Variability of JJAS Rainfall

The spatially averaged JJAS rainfall anomaly time series for Ethiopia (**Figure 3**) below demonstrates pronounced interannual variability throughout the 1981-2023 period. Alternating wet and dry years reflect that the regions are strongly sensitive to large-scale climate drivers. Persistent negative anomalies dominate parts of the 1980s and early 1990s, consistent with widespread drought conditions characteristic of those decades. On the other hand, the post-2001 period shows slightly more frequent positive anomalies, and variability remains high with a clear regime shift, emphasizing the need to assess evolving teleconnection influence on Ethiopia's summer rainfall.

The applied 3-year running mean indicates that the presence of low-frequency fluctuations superimposed on strong year-to-year variability shows that rainfall tends to cluster into short wet and dry episodes rather than exhibiting continued long-term regimes. The linear trend shows a moderate increase in JJAS rainfall, approximated as 8.3 mm per decade. By contrast, this trend is weak compared to the magnitude of interannual variability, highlighting the dominant role of short-term climate modes such as ENSO.

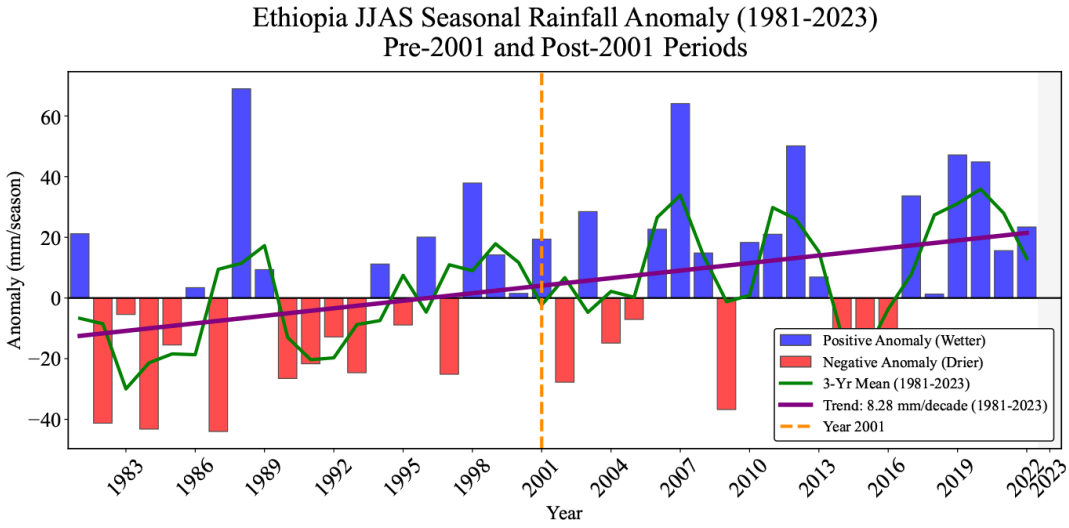

Figure 3. JJAS seasonal rainfall anomalies for 1981-2023 relative to the 1991-2020 climatology. Positive (wet) and negative (dry) anomalies are shown as blue and red bars, respectively, with a 3-year running mean linear trend overlaid (green). The vertical (orange) dashed line marks the point of climate shift, and the purple solid diagonal line indicates the trend.

3.3. Decadal Evolution of ENSO-JJAS Rainfall Teleconnection

Figure 4 describes the running correlation between JJAS rainfall over Ethiopia and ENSO (Niño 3.4 index) using (8, 10, 12, and 15) year moving windows for 1981-2023. Across all window sizes, the correlations demonstrate a clear decadal shift in the ENSO-rainfall relationship, indicating a teleconnection change in pathways affecting the Ethiopian summer monsoon. During the 1980s and 1990s, all windows showed strong negative correlations consistently exceeding −0.7 across all running window lengths, demonstrating that El Niño events were strongly associated with suppressed JJAS rainfall, while La Niña tended to enhance precipitation. The ENSO-rainfall association systematically moves toward weaker negative values starting in the late 1990s, with a noticeable shift around 2001.

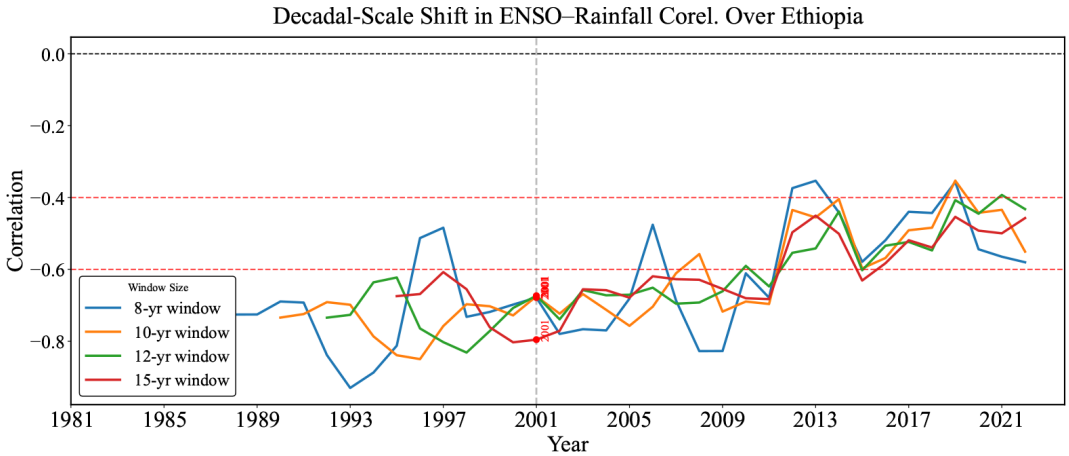

Figure 4. Decadal-scale evolution of the ENSO-rainfall correlation (sliding-window), using 8, 10, 12, and 15-year windows (colored curves). Horizontal dashed red lines denote reference correlation thresholds (−0.4 and −0.6), and the vertical grey dashed line highlights the transition period (2001).

Correlations stabilize at close to r = −0.4 to −0.5 for all window lengths in the post−2001 period. The ENSO signal's decadal decline indicates that Ethiopian JJAS rainfall has become less sensitive to ENSO forcing in recent decades. This decadal weakening of the ENSO teleconnection is statistically supported by a Monte Carlo Pettitt non-parametric change-point detection test applied to the 10-year running correlation series, which identifies a significant break point in 2001 (p = 0001). This provides an objective justification for dividing the study period into early and recent periods. The transitions is consistent across all running window lengths (8 - 15 years), confirming that change represents a true regime shift rather than sampling variability. Ethiopian JJAS rainfall has generally been less responsive to ENSO forcing in recent decades, indicating a strong weakening of the teleconnection, according to the running correlations and the Pettitt test results.

3.4. Co-Evolution of ENSO and JJAS Rainfall

Figure 5(a) illustrates the co-evolution of normalized JJAS precipitation anomalies across Ethiopia and the Niño 3.4 SST index for 1981 to 2023. The Ethiopian JJAS rainfall anomalies indicate strong yearly variation, with several extreme wet and dry seasons. The Niño 3.4 index alternates between warm (El Niño) and cool (La Niña) phases. The rainfall deficits generally coincide with El Niño events, and surpluses with La Niña, particularly in the earlier part of the record. The result indicates that the rainfall and Niño 3.4 index have a statistically significant negative correlation in both periods. But the weakness declines from r = −0.71 ($p < 0.001$) in 1981-2001 to r = −0.59 (p = 0.004) in 2002-2023. These p-values indicate the statistical significance of the ENSO-rainfall correlation within each respective sub-period. To explicitly test whether this weakening represents a statistically significant change between the two periods, we applied a Fisher r-to-z transformation. The result shows that the difference between the early and recent correlation coefficients is not statistically significant (z= −0.61, p = 0.54), suggesting that ENSO teleconnection weakening occurs gradually rather than as an abrupt step change between the two fixed sub-periods.

Figure 5(b) indicates the historical progression of ENSO's influence on Ethiopia's JJAS rainfall using a 10-year sliding window correlation. The sliding window correlation, which consistently remains negative throughout the analytic period, confirms the ongoing unfavorable relationship between ENSO warm events and Ethiopian summer rainfall. However, the magnitude of this correlation changes substantially. The late 1980s and early 1990s indicate the strongest negative correlations (r −0.71), suggesting a period of increased ENSO sensitivity. Although still statistically significant, the correlation weakens after 2001, with a number of years exhibiting values closer to −0.59. Wider confidence intervals indicate greater unpredictability and uncertainty. Importantly, formal change point identification has additional evidence for this temporal weakening. A Monte Carlo Pettitt test applied to the running correlation series identifies a highly significant regime shift

in 2001 (p = 0.0001), providing objective evidence that the ENSO-rainfall teleconnection has undergone a robust structural change rather than reflecting sampling variability.

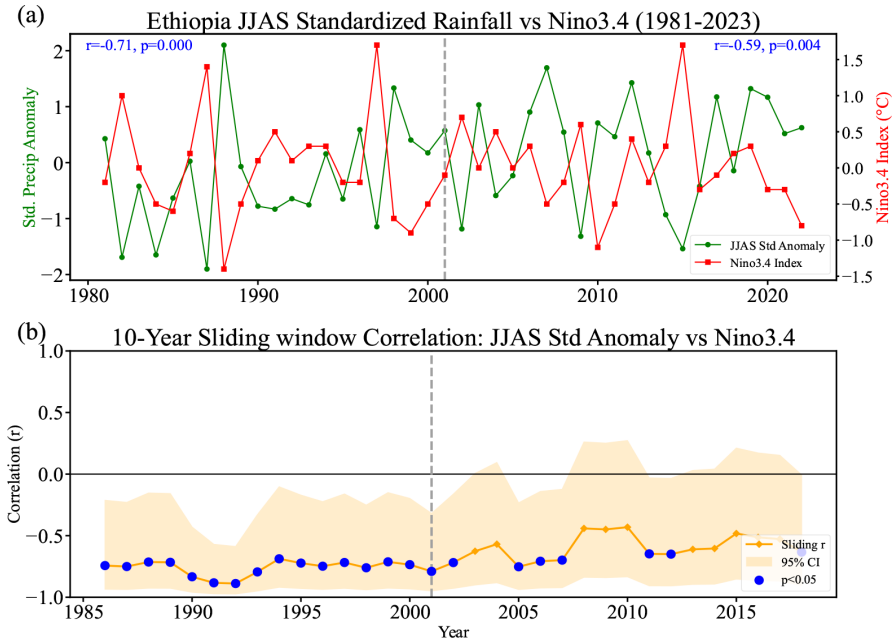

Figure 5. (a) Correlation of standardized JJAS precipitation anomalies and the Niño 3.4 SST index, (b) ten-year sliding window correlations between JJAS rainfall anomalies and Niño 3.4, with the shaded 95% confidence intervals (blue dots). The vertical dashed (black) line indicates the transition period around 2001.

3.5. Clustering of ENSO-Driven JJAS Rainfall Responses

Figure 6(a) illustrates the regional distribution of relationships between ENSO and JJAS rainfall over Ethiopia. A strong negative correlation in the central and northern regions indicates a strong and consistent ENSO signal, with reduced rainfall during El Niño and increased rainfall during La Niña. In the western region, correlations are still negative but weaker and more spatially variable, indicating a less consistent ENSO influence. Similar weak to moderate negative correlations are seen in the southwest, suggesting that JJAS rainfall is not very sensitive to ENSO impact. The southeast, on the other hand, exhibits weak positive correlations, revealing a unique regional response within the ENSO-rainfall correlation and showing a tendency toward slightly enhanced rainfall during El Niño episodes. **Figure 6(b)** further indicates that the spatial reorganization of ENSO sensitivity occurs in four different zones. The presence of four distinct, geographically stable clusters suggests that the effects of ENSO have not only intensified in some areas but also become more clearly defined. The central and northeastern regions have been covered by Cone A, which shows the place with the most negative correlation in **Figure 6(b)**, indicating these areas have experienced high rainfall suppression as a result of ENSO. While Zone C, which is characterized by negative correlations, now includes places that previously

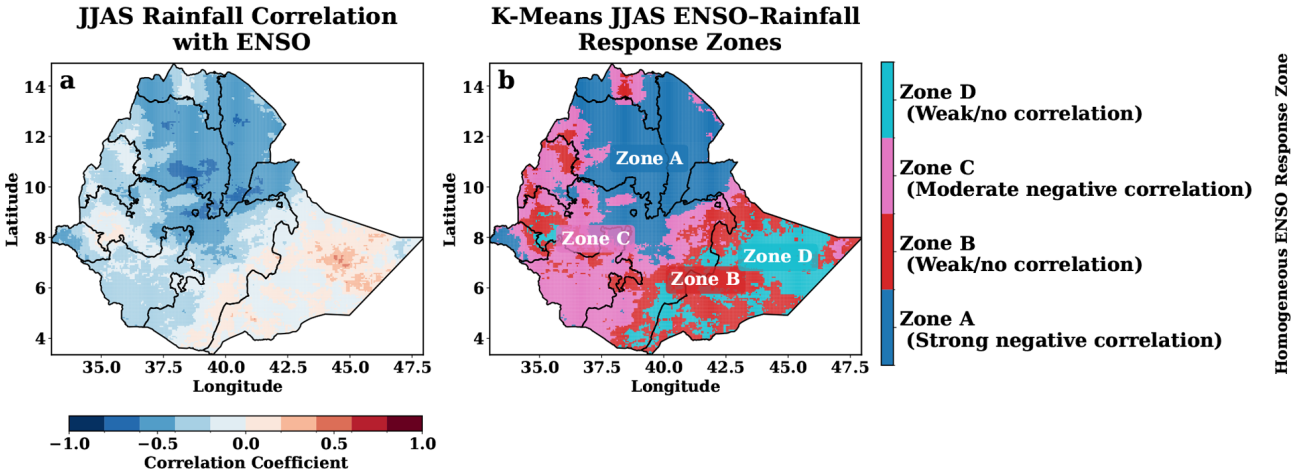

Figure 6. JJAS rainfall correlation with ENSO and corresponding response zones. (a) Spatial correlation between JJAS and ENSO, (b) K-means clusters identifying homogeneous ENSO-rainfall response zones; Zone (a) strong negative, Zones (b and d) weak or no correlation, Zone (c) moderate negative correlations.

showed significant ENSO sensitivity, indicating changes in teleconnection pathways, Zones B and D indicate areas where JJAS rainfall variability is minimal and independent from ENSO influence.

3.6. Changes in ENSO Impacts in Recent Decades

Figure 7(a)-(f) describes the spatial distribution of rainfall anomalies, highlighting both the 1981-2001 and 2002-2023 periods. These figures provide insight into region-specific patterns, revealing how rainfall has varied over time and space. In addition, by comparing these periods and their anomalies, the analysis highlights climatologically significant JJAS rainfall zones, providing a better understanding of both previous and recent trends in Ethiopian summer rainfall, emphasizing areas that are particularly sensitive to ENSO-related variability.

Figure 7(a) illustrates that the composite precipitation anomalies during the El Niño year show that Central and northwestern Ethiopia experienced negative anomalies, exceeding −20 mm/month, revealing strong drought conditions. Meanwhile, southwestern, eastern, and pockets of northern regions show weak positive anomalies, indicating slightly wetter than average conditions. In the later period, Figure 7(b) shows negative anomalies over central Ethiopia remain strong; on the other hand, western Ethiopia shows a decrease in drought intensity relative to the earlier period. Figure 7(c) shows that positive rainfall anomalies occurred over the western parts of Ethiopia, while the northeastern, eastern, and southwestern parts of the country showed negative rainfall anomalies.

Figure 7(d) illustrates that precipitation anomaly during La Niña years; positive anomalies dominate central, western, and southern Ethiopia, remaining stable with enhanced summer rainfall during La Niña events, while the southwestern and northeastern regions experience slightly negative anomalies. These findings strengthen previous studies, highlighting La Niña as a factor for above normal JJAS rainfall in the Ethiopian highlands, supporting its role as a critical driver of

interannual rainfall variability. Figure 7(e) shows La Niña years with wet anomalies persisting over most parts of the country, while southwestern Ethiopia experiences weak negative to neutral anomalies. Figure 7(f) illustrates the difference map, highlighting a weakening of La Niña-induced wet anomalies in the central and western parts of Ethiopia, while an increase in rainfall anomalies occurs over the southwestern and northeastern regions, which indicates a southwestward and northeastern regional shift in La Niña influence.

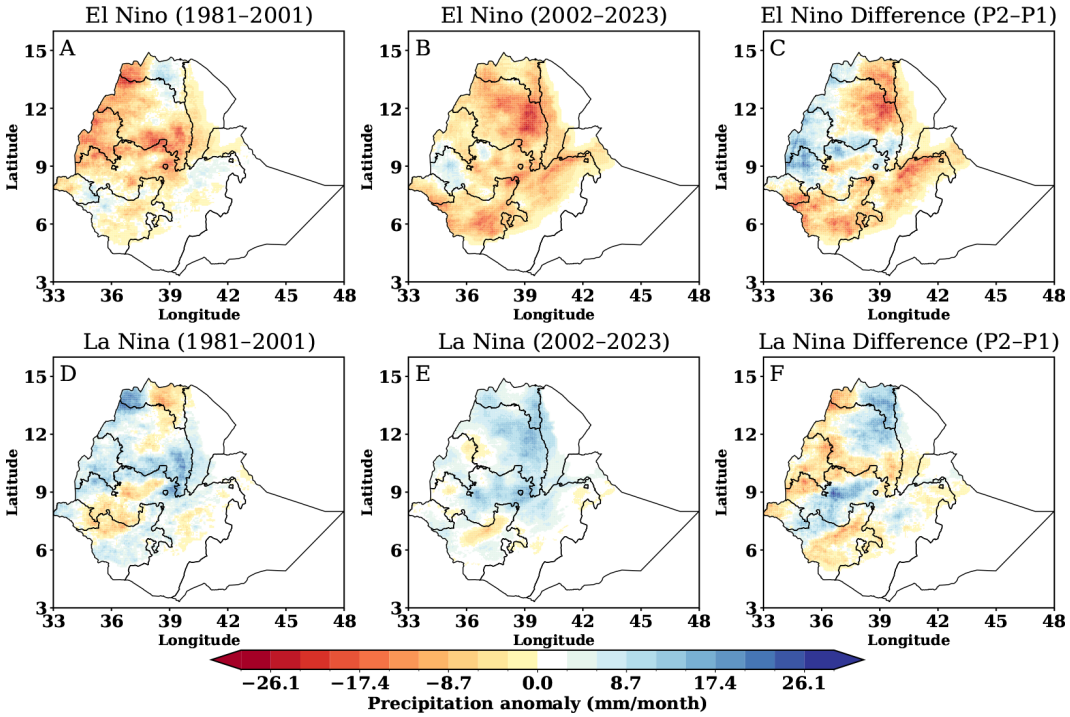

Figure 7. Spatial patterns of ENSO-related JJAS rainfall anomalies. (a)-(c) Precipitation anomalies during El Niño events for (1981-2001) and (2002-2023), and the difference. (d)-(f) Corresponding anomalies for La Niña events and the difference. Shading indicates rainfall anomalies (mm·season^{-1}) with colors representing deviation from the climatological mean.

3.7. Non-Stationary Spatial ENSO-Summer Rainfall Relationship

Figure 8(a)-(i) illustrates non-stationarity in the spatial relationship between ENSO and JJAS rainfall for the two analysis periods. During 1981-2001, correlation patterns indicate a predominantly negative association between Niño 3.4 and rainfall across the western, central, northern, and southwestern highlands, with statistically significant correlations (−0.4 and −0.7), indicating that El Niño events were consistently linked to suppressed summer rainfall. On the other hand, the eastern and southeastern lowlands

Regions show weak to moderate positive correlations, highlighting the well-established spatial heterogeneity of ENSO influence and corresponding with canonical teleconnection mechanisms affecting Ethiopian summer rainfall.

In the later period, 2002-2023, the spatial coherence of ENSO-rainfall coupling weakens, and correlation changes across large portions of the country. The north-

western regions, which previously showed strong negative correlation, now display weak positive correlations, in some cases exceeding +0.3. Central Ethiopia likewise experiences substantially weakened correlations, while southern and southeastern regions show a weak positive correlation. Statistical significance becomes limited across the domain, indicating that ENSO has become a notably less sound predictor of JJAS rainfall variability. The difference map underscores the scale of this reorganization; large positive anomalies dominate the southwestern and western regions, demonstrating a shift from robust ENSO-induced drying to ENSO-associated wetness in recent decades.

Regression slope patterns in Figure 8(d)-(f) also strengthen this shift. During 1981-2001, strongly negative slopes prevailed across the western and northern highlands, in some areas exceeding −8 to −12 mm·month^{-1} per standard deviation of Niño 3.4, confirming that El Niño events historically exerted a physically meaningful drying influence on seasonal rainfall totals. By contrast, the later period Figure 8(e) shows a marked weakening of these sensitivities. The explained

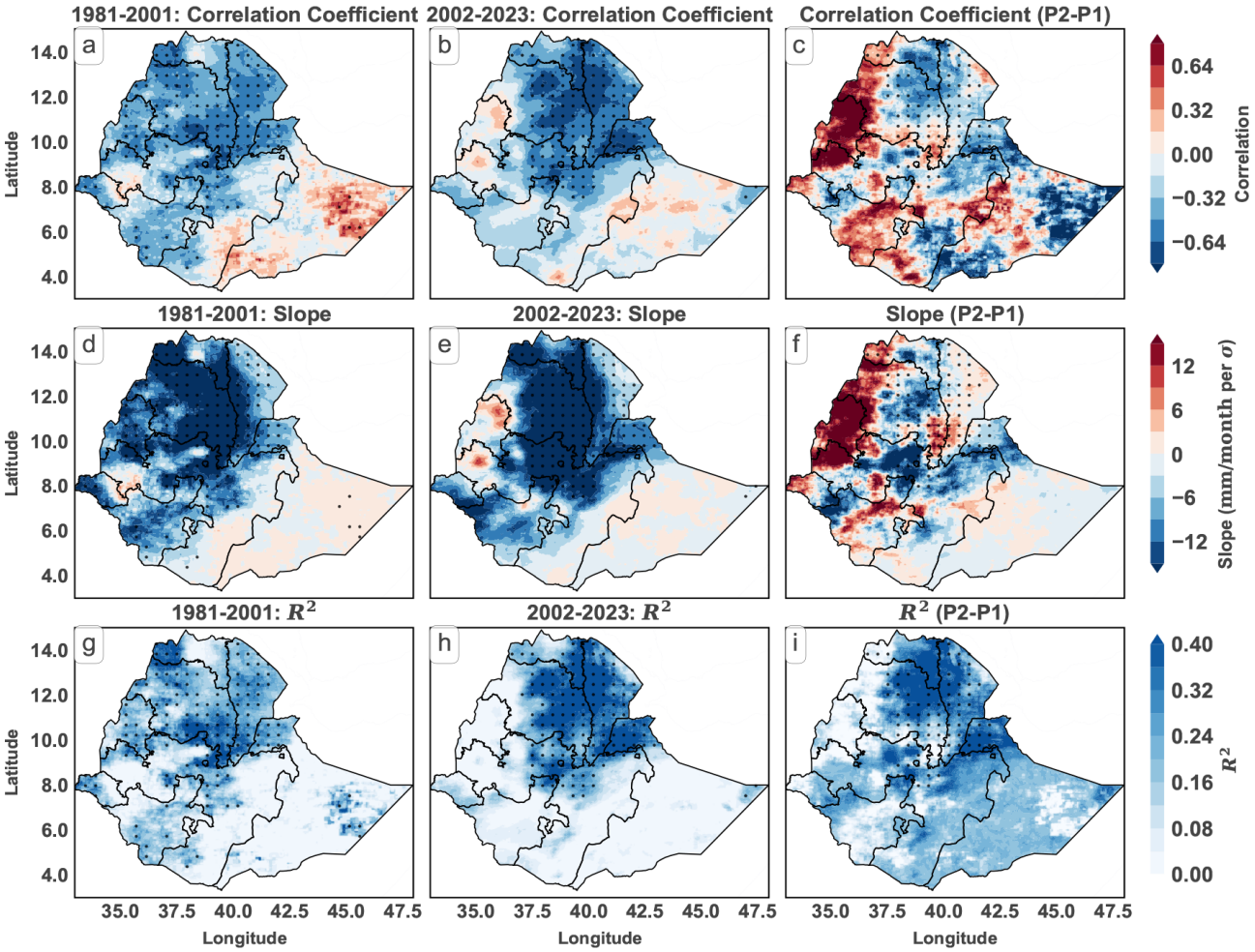

Figure 8. Spatial evolution of the ENSO-JJAS rainfall teleconnection over Ethiopia for two time periods (1981-2001) and (202-2023). Figure (a)-(c) presents Pearson correlation coefficients, (d)-(f) regression slopes (mm·month^{-1} per standard deviation), and their differences (P2-P1). Black dots denote locations with statistically significant relationships at $p < 0.05$.

variance (R^2) further demonstrates that ENSO's influence on most summer rainfall has declined from 30% - 40% of rainfall variance in the earlier periods to generally below 10% after 2001 across most regions of the country. The overall result demonstrates that ENSO-summer rainfall teleconnections over Ethiopia have weakened, reorganized, and locally reversed.

3.8. Moisture Flux Divergence Anomaly at 850 hPa

The spatial patterns of JJAS moisture flux divergence (MFD) anomalies and rainfall differences between the two study periods reveal clear evidence that ENSO-related moisture pathways that influence Ethiopia have undergone substantial reorganization in recent decades. During the earlier period (1981-2001), the MFD anomalies exhibit a distribution consistent with the well-documented earlier teleconnection in which ENSO-related circulation responses modulate the cross-equatorial flow and moisture supply toward the Ethiopian highlands. Strong and spatially dense moisture convergence appears over parts of central and northern Ethiopia, while divergence is concentrated over southern and southeastern regions. This pattern suggests that ENSO primarily influenced Ethiopian rainfall through upper-level subsidence and low-level convergence anomalies, rather than through a major reorganization of monsoon inflow.

By contrast, the anomaly pattern for 2002-2023 demonstrates a notable intensification and reorientation of low-level moisture circulation. Large areas of the Ethiopian highlands, especially in the eastern and northeastern regions, have recently been characterized by strong moisture divergence accompanied by enhanced anomalies of easterly and northeasterly moisture fluxes that penetrate inland from the Arabian Sea. These changes are consistent with a strengthened ENSO influence on large-scale Pacific atmospheric circulation, with increased sensitivity to El Niño events that have become more frequent since early 2001. The altered Walker and Hadley circulation responses linked to Pacific warming suppress moisture transport toward Ethiopia, resulting in reduced near-surface moisture availability over the region and a tendency for anomalous moisture convergence to shift away from Ethiopia.

The anomaly difference field **Figure 9(c)** highlights a coherent enhancement of moisture divergence over Ethiopia, and strengthened early inflow from the Gulf of Aden underscores a structural change in the low-level monsoon response to ENSO. This reorganization is consistent with Favors' offshore or zonally deflected moisture transport rather than cross-equatorial westerlies feeding the highlands. In association with this, the rainfall difference **Figure 9(d)** illustrates widespread drying over eastern and northeastern Ethiopia (decrease of 70-150 mm), spatially aligned with intensified moisture divergence, finding supported by (Endris et al., 2019) showing that ENSO teleconnections over Ethiopia have shifted as changes in Pacific SST gradients and warming patterns have evolved, leading to altered Rossby wave propagation and changes in the Walker circulations. The difference map reveals a teleconnection regime in which ENSO more effectively modulates near-surface moisture pathways, producing a tangible decline in moisture conver-

gence over Ethiopia. On the other hand, southern Ethiopia experiences increased rainfall due to southward shifted convergence zones.

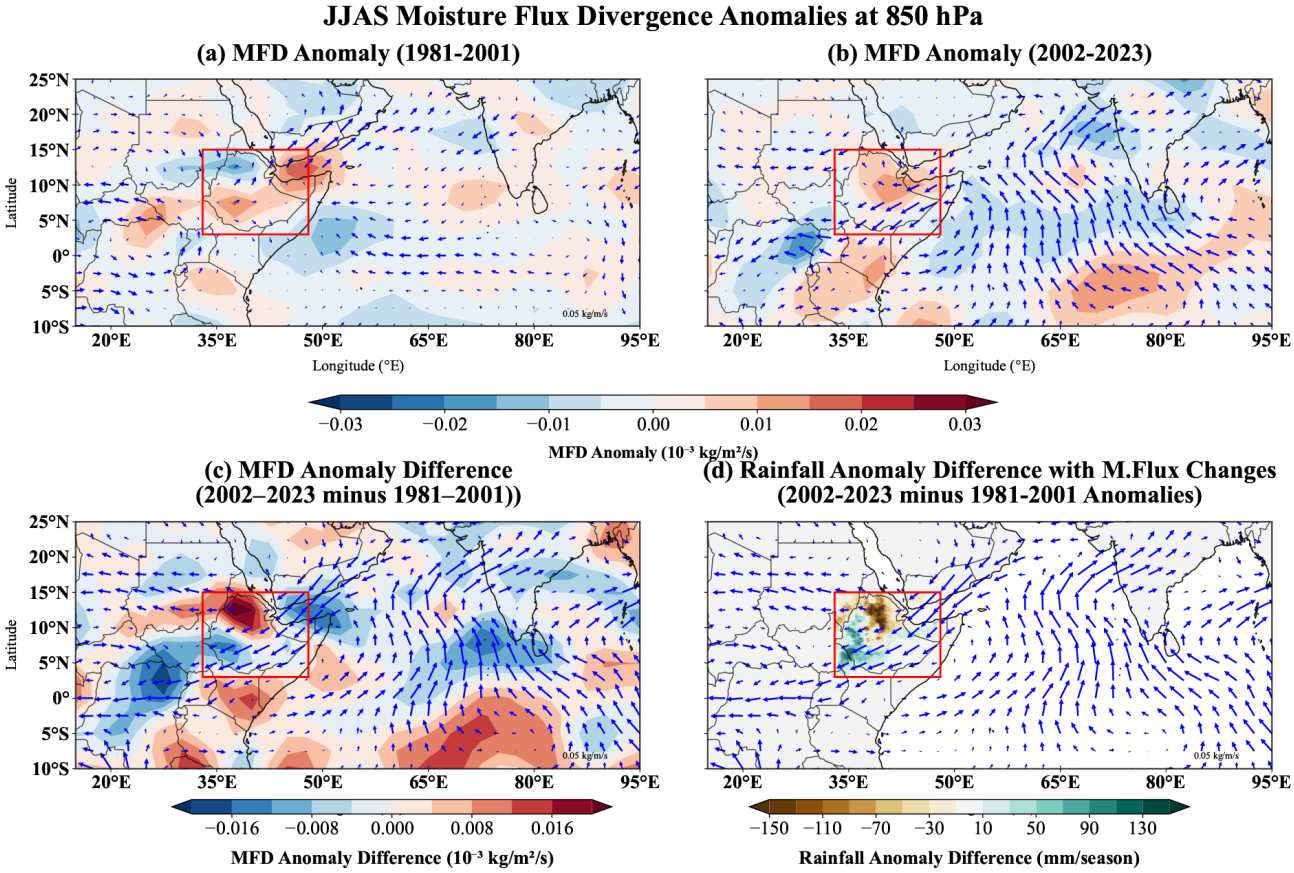

Figure 9. JJAS moisture flux divergence (MFD) anomalies and precipitation difference between 1981-2001 and 2002-2023. Figure (a)-(b) 850 hPa MFD anomalies for each period, (c) MFD differences, (d) rainfall difference with moisture flux anomaly. Warm colors indicate divergence or rainfall decrease; cool colors indicate convergence or increase. The Ethiopian domain is outlined in red.

3.9. Vertical Circulation Response to ENSO Phases

Figure 10 presents a zonal vertical cross-section of composites of anomalous vertical motion (ω) and zonal wind for El Niño and La Niña events across the two periods (1981–2001) and (2002–2023). The composites highlight the dynamic processes by which ENSO impacts Ethiopian JJAS rainfall and illustrate how this influence has changed. During 1981–2001, El Niño conditions were associated with anomalous subsidence over Ethiopia (Figure 10(a)), particularly in the mid-troposphere, consistent with the canonical ENSO-driven suppression of convection and reduced JJAS rainfall. This circulation structure reflects a relatively coherent ENSO-rainfall coupling during the earlier period.

In the more recent period (2002–2023), El Niño-related anomalies remain detectable (Figure 10(b)); however, the subsidence signal appears less consistently centered over Ethiopia's main rainfall-producing region and shows a more spatially heterogeneous structure. Although localized mid-level sinking persists, the

overall overturning response does not translate into a uniformly stronger drying impact. This suggests that ENSO-driven vertical circulation has become less efficiently coupled to JJAS rainfall variability, consistent with the observed weakening of El Niño's influence in Ethiopian drought conditions. The difference pattern (Figure 10(c)) further highlights this reorganization, indicating that the recent El Niño circulation anomalies are characterized more by shifts in vertical structure and displacement of subsidence rather than a systematic intensification of drying over Ethiopia.

Figure 10(d) and Figure 10(e) describe the La Niña anomalies. During the early period, La Niña produced modest ascent and low-level convergence, consistent with relatively moderate wet anomalies. In contrast, the recent period indicates a more coherent ascent extending through a deeper layer of the troposphere, along with enhanced low-level inflow and upper-level divergence. These features suggest that La Niña's moistening influence has become relatively more pronounced after 2001.

Overall, Figure 10 illustrates a clear reorganization of ENSO-driven circulation patterns over Ethiopia. While ENSO-related vertical motion anomalies remain present, their spatial structure and coupling with regional moisture have changed.

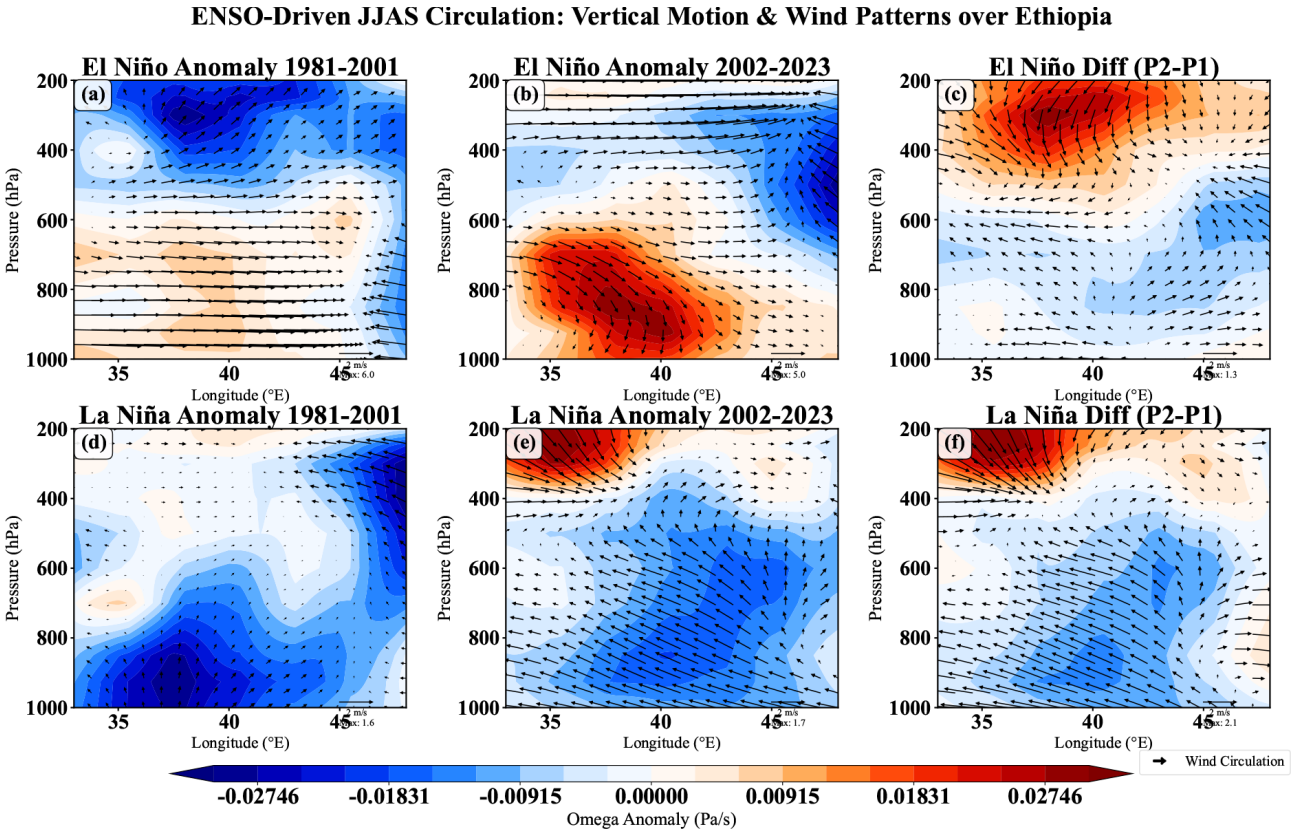

Figure 10. Longitude-pressure cross-section of ENSO-driven JJAS circulation anomalies. The shaded contour shows vertical velocity (ω) anomalies (Pa·s^{-1}), with negative (blue) values indicating anomalous ascent and positive (red) values indicating anomalous subsidence. Vectors represent zonal vertical wind anomalies. (a)-(c) show El Niño anomalies and the difference between the two periods. (d)-(f) show La Niña anomalies and differences.

In particular, the altered positioning and heterogeneity of El Niño-induced subsidence reduce its effectiveness in suppressing JJAS rainfall, consistent with the observed weakening of ENSO's drying impact in recent decades.

3.10. ENSO-Rainfall Lead Time Relationship

Figure 11(a)-(d), 1981-2001 periods, the spatial pattern shows clear lead-time dependence in the correlation between ENSO and regional climate variability. At longer lead times (12 and 6 months), correlations are generally weak and spatially scattered, indicating a limited predictive influence of ENSO far in advance. As the lead-time shortens to 3 months, a well-defined strengthening of the signal appears, with statistically significant correlations developing across large parts of northern, central, and eastern Ethiopia. The strongest and most spatially coherent correlations are seen at zero-month lead, especially over the northern highlands, where this strengthening peaks. During this period, ENSO influences are dominated by short-lead mechanisms, reflected in the gradual transition from weak long-lead signals to stronger short-lead responses. The influence of ENSO is greatest when its conditions occur simultaneously with regional climate variability.

On the other hand, (Figure 11(f)-(h)), the 2002-2023 period demonstrates a noticeably weaker and less coherent lead-time evolution. At 12- and 6-month leads, correlations remain weak and spatially unpredictable, similar to the earlier period but with reduced magnitude. Even though correlations increase at the 3-month lead, the spatial magnitude and intensity of significant correlations are

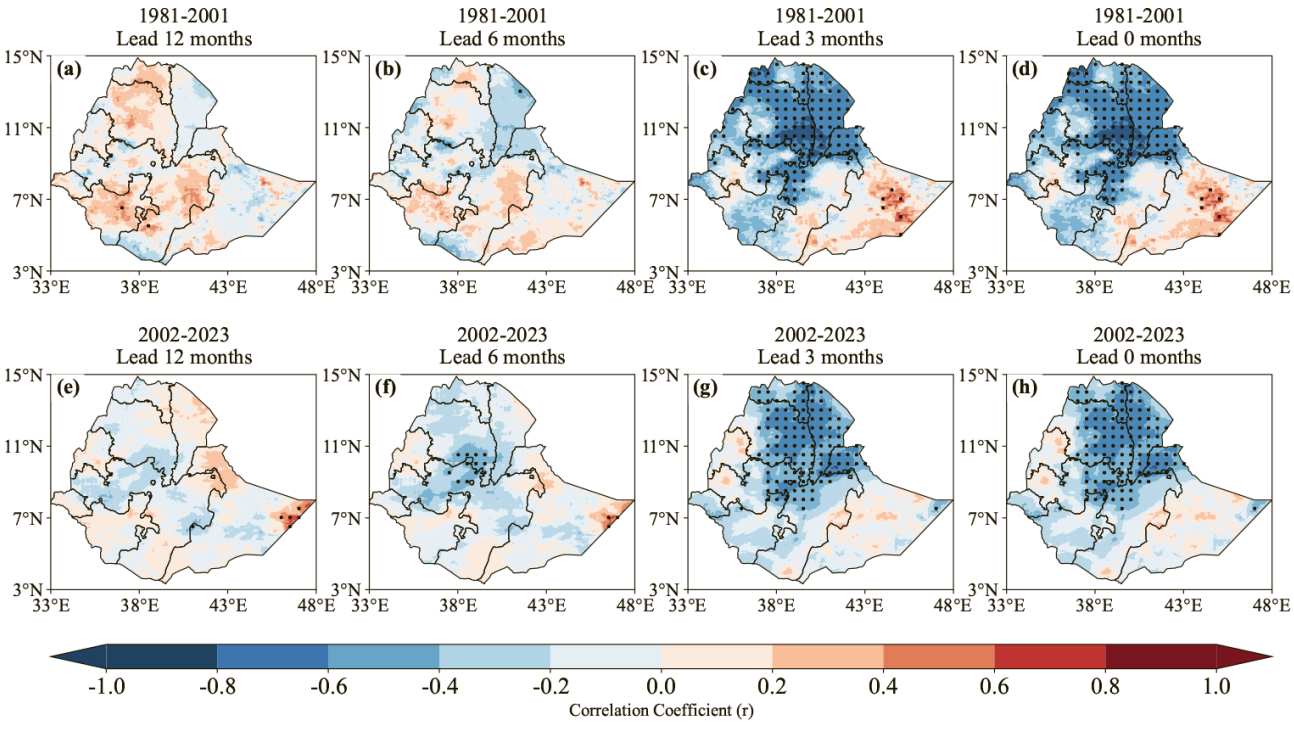

Figure 11. Spatial correlation between the ENSO index and JJAS rainfall over Ethiopia at 12-, 6-, 3-, and 0-month lead times, for the 1981-2001 periods (a)-(d) and for 2002-2023 (e)-(h). Stippling denotes correlations significant at the 95% confidence level.

smaller compared to 1981-2001. At zero-month lead, the ENSO signal appears more localized and less robust, with reduced spatial coverage over Ethiopia. This weakened short-lead response reflects a reduced sensitivity of regional climate to ENSO forcing in the recent period, suggesting a decline in ENSO-related predictability at lead times where the strongest responses were previously observed.

3.11. ENSO-Conditioned Drought and Flood Frequency

ENSO-conditioned drought and flood frequency demonstrate significant variations between the two study periods, revealing a clear weakening of ENSO rainfall teleconnections over Ethiopia. During 1981-2001, El Niño years Figure 12(a) & Figure 12(b) are characterized by widespread drought frequency across the northwest, central, eastern, and Rift Valley regions, with drought frequency exceeding 30% of the El Niño JJAS season in most areas. Flood occurrences remained low and are spatially confined to isolated pockets, underscoring the well-established association between warm ENSO events and suppressed summer rainfall. In contrast, the La Niña years' Figure 12(e) & Figure 12(f) shows an opposing pattern: drought frequencies and excessive flooding, often exceeding 25% - 30%, dominate the western, northern, and southeastern highlands. These spatial signatures reflect a strong and coherent ENSO influence during 1981-2001.

For the period 2002-2023, ENSO-related extremes become more heterogeneous. Under El Niño Figure 12(c) & Figure 12(d), drought frequency persists in the northern, northeastern, and central southwestern regions, but their magnitude is more variable and spatially fragmented compared to the earlier period. Some areas in the south and southwest, which previously indicated limited El Niño-related drought influence, now display moderate drought occurrences, indicating a potential southward expansion of ENSO impacts. Flood frequency during El Niño year's remains generally low but becomes more spatially dispersed, indicating weakened consistency in the atmospheric response to warm ENSO phases. La Niña years in 2002-2023 Figure 12(g) & Figure 12(h) continue to be associated with elevated flood frequency, particularly in northern and southwestern highlands, with high intensities. Notably, drought occurrence during La Niña appears slightly more widespread in the northern and northeastern regions, pointing to a weakening of the previously strong wetting influence of La Niña in these regions.

Figure 12(i)-(j) indicates that drought occurrence increases markedly across central and eastern Ethiopia**,** with localized enhancements extending into the northern highlands, while parts of western and southwestern Ethiopia exhibit weak or negative changes. In contrast, El Niño-related flood frequency generally declines over much of the country, indicating a reduced contribution of El Niño events to wet extremes in the recent period, and shows a strengthening of El Niño-driven dry extremes and a concurrent weakening of flood-producing conditions after 2001. Figure 12(k)-(l) depicts changes associated with La Niña events, revealing an opposing signal. Drought frequency decreases across most regions, while flood frequency increases, with pronounced enhancements in the south and southeast. This coherent spatial response indicates an intensification of La Niña-related wet

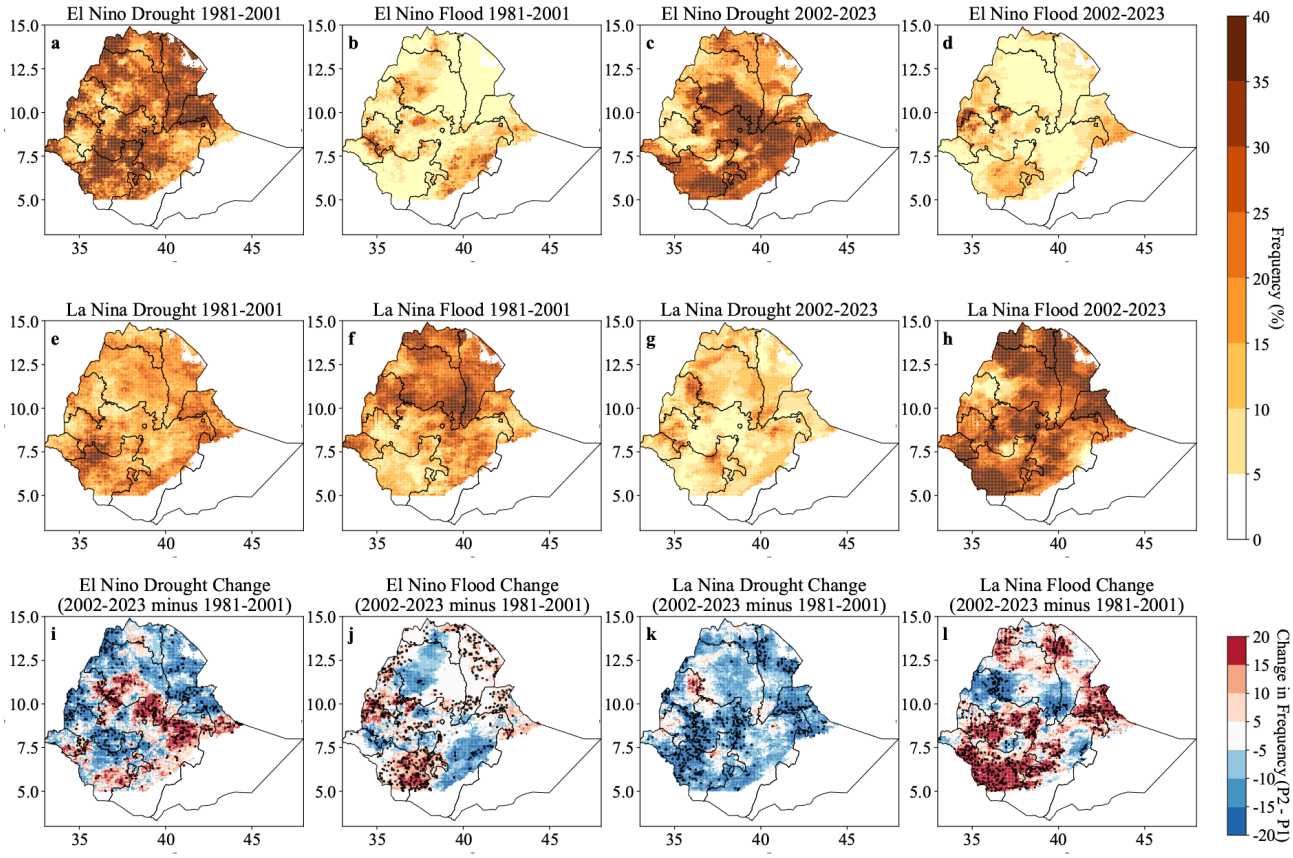

Figure 12. ENSO-related drought and flood frequency for 1981-2001 and 2002-2023, and their inter-period changes. (a)-(d) show El Niño drought and flood frequencies for the two periods; (e)-(h) show the corresponding La Niña frequencies. Figure (i)-(l) shows changes in drought and flood frequency (2002-2023 minus 1981-2001). Frequencies are expressed as percentages, and stippling indicates grid cells with significant inter-period differences at the 95% level.

conditions in recent decades.

3.12. AMO-Driven Teleconnections Shift

Figure 13(a) and Figure 13(b) indicates the spatial correlation analyses, indicating a significant shift in large-scale climate controls on Ethiopia's JJAS rainfall between 1981-2001 and 2002-2023. Ethiopian JJAS rainfall and the Atlantic Multidecadal Oscillation (AMO) have a weak and regionally negligible correlation in the earlier decades (1981-2001). Northern and northeastern Ethiopia indicate moderate positive correlation, while southern and southeastern regions exhibit negative signals, indicating minimal AMO influence on the summer monsoon. This pattern corresponds with the 1980s-1990s climate regimes, when ENSO dominated Ethiopian rainfall variability and largely controlled drought and flood occurrence.

A notable change emerges in the spatial correlation patterns for the period 2002-2023. During these periods, strong and statistically significant positive correlations between the AMO and JJAS rainfall develop across northern, central, eastern, and western Ethiopia; stronger negative correlations appear in the southeast parts of the country. This transformation indicates that the AMO has become

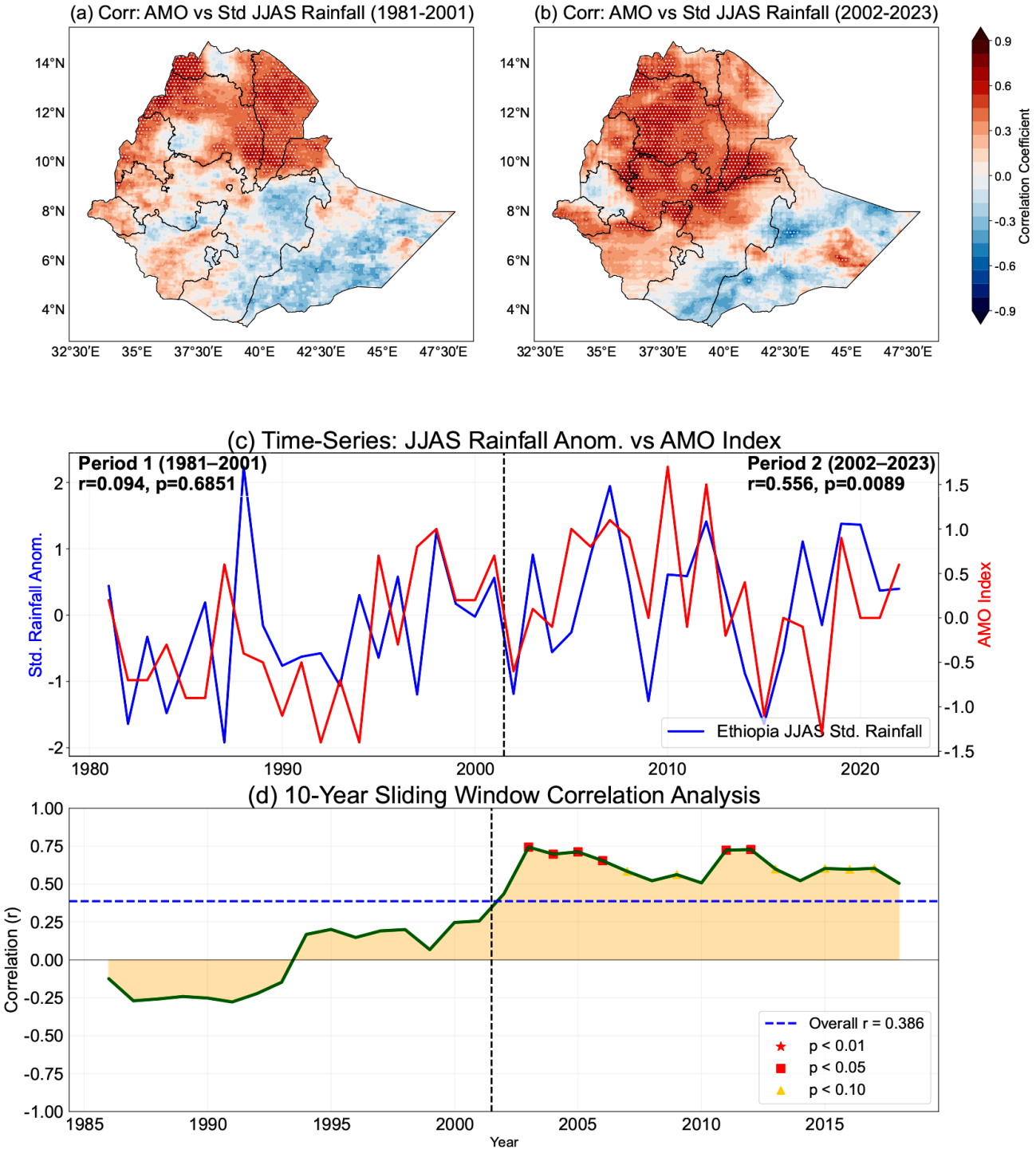

Figure 13. Spatial correlation between the Atlantic Multidecadal Oscillation (AMO) and standardized JJAS rainfall (a) 1981-2001 and (b) 2002-2023 periods respectively. The dotted lines highlight statistically significant regions ($p < 0.05$). (c) Shows the time series of standardized rainfall anomalies (blue) and AMO (red). (d) Indicates the 10-year sliding window correlation. The dashed blue line shows the overall correlation ($r = 0.386$), and the vertical dashed line indicates the shift between the two periods.

a major modulator of Ethiopia's rainfall regime in recent decades. The AMO's role in determining ENSO behavior and multi-basin circulation, and its developing impacts, suggest that ENSO influence is increasingly filtered through the Atlantic back-

ground state and modifies its magnitude, spatial expression, and predictability.

Physically, this enhanced AMO impact can be explained through large-scale atmospheric bridge mechanisms linking Atlantic SST anomalies to East African hydroclimate. During positive AMO phases, basin-wide warming of the North Atlantic strengths deep convection and enhances diabatic heating over tropical Atlantic. This anomalous heating excites stationary Rossby wave trains that propagate eastward across North Africa into the Afro-Asian regions, modifying upper level divergence and mid-tropospheric circulation over Ethiopia. At the same time, AMO-related warming alters the Walker and Hadley circulation cells, promoting subsidence over the central Atlantic and enhanced ascent over eastern Africa during JJAS season. This circulation adjustments strengthen the low-level westerly and southwesterly moisture from the Atlantic and Congo Basin toward the Ethiopian highlands, reinforcing JJAS rainfall over northern and western Ethiopia, while suppressing rainfall over southeastern regions through enhanced subsidence and moisture divergence (Yang et al., 2020).

The time series **Figure 13(c)** & **Figure 13(d)** further supports this physical interpretation. JJAS rainfall anomalies and the AMO index had a weak and statistically insignificant correlation between 1981 and 2001, indicating a weak Atlantic influence on Ethiopian JJAS rainfall. However, the relationship between Ethiopian rainfall and AMO has become statistically significance after 2001.This shift suggests that Ethiopia's JJAS rainfall has transitioned into a more complex climate regime and multi-ocean forcing system. The 10-year sliding window correlations **Figure 13(d)** analyses emphasize the timing of this climatic transition. Throughout the early periods, sliding window correlations between the AMO and JJAS rainfall remain near zero or at weak negative values. Beginning in the late 1990s, correlations gradually increase, exceeding 0.5 after 2001, and windows become statistically significant. All spatial, time series, and sliding window results indicate a regime shift in which ENSO remains influential but no longer acts alone; instead, coupled AMO interactions play a central role in governing JJAS rainfall variability.

4. Summary and Conclusion

This study provides robust evidence that Ethiopia's JJAS rainfall teleconnections have undergone substantial reorganization over recent decades. Using CHIRPS rainfall, ERA5 atmospheric fields, Niño 3.4, and AMO indices, this multi-dataset research finds a clear structural shift in the primary climate determinants influencing Ethiopian JJAS rainfall.

During the early period (1981-2001), ENSO exhibited a strong, spatially coherent teleconnection pattern. El Niño events are consistently linked to suppressed rainfall, and La Niña is associated with enhanced rainfall across central, northeastern, northwestern, and southwestern highlands. These results align with established mechanisms in which El Niño weakens monsoon flow, reduces low-level moisture transport, and strengthens subsidence over Ethiopia. Composite analyses and rainfall anomaly patterns in this study confirm this classical behavior in

the earlier decades.

However, evidence from this study indicates that after 2001, ENSO's influence has considerably weakened. Sliding window correlation demonstrates a clear decadal decline in ENSO rainfall correlation, with the correlation coefficient decreasing from r = −0.71 to r = −0.59. Windows have demonstrated weak, fragmented, or statistically insignificant correlations over the most recent 15-21 years. Regions previously displaying strong ENSO sensitivity, particularly the northwest and Rift Valley highlands, now experience much weaker teleconnections. Trend analysis of rainfall anomalies and regional clustering supports this shift by showing that most of Ethiopia's coherent rainfall regions weakly to moderately respond to ENSO phases inconsistently. ENSO-related moisture flux, divergence, and circulation anomalies are notably weaker in recent decades, showing disruption of historical Walker circulation pathways.

Composite moisture divergence patterns reveal less structured moisture export during El Niño events, which explains the decreased rainfall anomalies observed in recent ENSO phases, even while La Niña-related moisture convergence over Ethiopia has declined. However, this study shows that the Atlantic Multidecadal Oscillation (AMO) has a greater influence on Ethiopia's JJAS rainfall, with correlations increasing from r = 0.094 to r = 0.556, particularly between 2002 and 2023. The central, northern, southern, and western halves of Ethiopia all exhibit stronger positive correlation with the AMO in recent decades, particularly during the warm phase. This influence is likely due to shifts in hemispheric SST gradients modifying large-scale circulation and monsoon strength. The simultaneous weakening of ENSO and strengthening of AMO signals point to a developing multi-basin control of Ethiopia's JJAS rainfall variability. These developing teleconnections carry important implications for hydro-climatic risk management. ENSO-based drought and flood predictability has declined, with reduced lead-time forecasting skill and less consistent extreme event occurrence.

In conclusion, Ethiopia's JJAS rainfall has shifted from a mainly ENSO-driven system to a more networked climate regime influenced by interactions between the Pacific and Atlantic Oceans. Seasonal forecasting frameworks must therefore move beyond an ENSO-only perspective and incorporate Atlantic climate variability to improve prediction skill and strengthen climate risk management under evolving global teleconnections.

Acknowledgements

First of all, I want to thank everyone who helped and encouraged me throughout this research. First and foremost, I would like to thank my supervisor **Prof. Chaoxia Yuan**, for her insightful guidance, endless assistance, and inspiration during this research. Unrestricted conversations, helpful feedback, and gentle monitoring were essential to this study's success. Along with that, **Mulualem Abera Waza** has my deepest gratitude for his extraordinary kindness, inspiration, and continuous support throughout the study, and we were very grateful for his

support and inspiration. Finally, I would like to thank **Nanjing University of Information Science and Technology** for providing the facilities and supportive research environment needed to complete this study.

Author Contributions

Prof. Chaoxia Yuan: Conceptualization, Project administration, Resources, Supervision, Methodology, Investigation, Formal analysis, Validation, Visualization, Writing - original draft, Writing - review & editing.

Addisu Belachew: Conceptualization, Methodology, Software, Data curation, Investigation, Formal analysis, Validation, Visualization, Writing - original draft, Writing - review & editing. Asaminew Teshome: Conceptualization, Validation, Writing - review & editing.

Mulualem Abera Waza: Conceptualization, Methodology, Software, Formal analysis, Visualization, Writing - review & editing.

Funding Information

This research received no specific grant from any funding agency in the public, commercial, or not-for-profit sectors.

Data availability:

1) CHIRPS precipitation data is available at https://data.chc.ucsb.edu/products/CHIRPS-2.0/global_monthly/netcdf/chirps-v2.0.monthly.nc.

2) Monthly Niño 3.4 index data were obtained from NOAA Physical Science Laboratory (https://psl.noaa.gov/data/timeseries/month/Nino34/).

3) Atmospheric circulation variables were obtained from ERA5 (https://cds.climate.copernicus.eu/datasets/reanalysis-era5-single-levels-monthly-means?tab=download) and,

5) Atlantic Multidecadal Oscillation (AMO) from (https://psl.noaa.gov/data/timeseries/AMO/).

6) SRTM elevation data is available at (http://srtm.csi.cgiar.org/wp-content/uploads/file/srtm_5x5/TIFF/).

7) Natural Earth Country boundaries are available at (http://www.naturalearthdata.com/).

Conflicts of Interest

The authors declare no conflicts of interest regarding the publication of this paper.

References

Arguez, A., Durre, I., Applequist, S., Vose, R. S., Squires, M. F., Yin, X. et al. (2012). NOAA's 1981-2010 U.S. Climate Normals: An Overview. *Bulletin of the American Meteorological Society, 93,* 1687-1697. https://doi.org/10.1175/bams-d-11-00197.1

Bayr, T., Lübbecke, J. F., Vialard, J., & Latif, M. (2025). Equatorial Pacific Cold Tongue Bias Degrades Simulation of ENSO Asymmetry Due to Underestimation of Strong Eastern Pacific El Niños. *Journal of Climate, 37,* 6167-6182. https://doi.org/10.1175/jcli-d-24-0071.1

Bell, B., Hersbach, H., Simmons, A., Berrisford, P., Dahlgren, P., Horányi, A. et al. (2021). The ERA5 Global Reanalysis: Preliminary Extension to 1950. *Quarterly Journal of the Royal Meteorological Society, 147,* 4186-4227. https://doi.org/10.1002/qj.4174

Camberlin, P. (2023). *Climate of Eastern Africa.* Oxford Research Encyclopedia of Climate Science. https://doi.org/10.1093/acrefore/9780190228620.013.512

Chen, L., Li, G., Lu, B., Li, Y., Gao, C., Long, S. et al. (2022). Two Approaches of the Spring North Atlantic Sea Surface Temperature Affecting the Following July Precipitation over Central China: The Tropical and Extratropical Pathways. *Journal of Climate, 35,* 2969-2986. https://doi.org/10.1175/jcli-d-21-1012.1

Degefu, M. A., Rowell, D. P., & Bewket, W. (2017). Teleconnections between Ethiopian Rainfall Variability and Global SSTs: Observations and Methods for Model Evaluation. *Meteorology and Atmospheric Physics, 129,* 173-186. https://doi.org/10.1007/s00703-016-0466-9

Diro, G. T., Grimes, D. I. F., & Black, E. (2011). Teleconnections between Ethiopian Summer Rainfall and Sea Surface Temperature: Part I—Observation and Modelling. *Climate Dynamics, 37,* 103-119. https://doi.org/10.1007/s00382-010-0837-8

Endris, H. S., Lennard, C., Hewitson, B., Dosio, A., Nikulin, G., & Artan, G. A. (2019). Future Changes in Rainfall Associated with ENSO, IOD and Changes in the Mean State over Eastern Africa. *Climate Dynamics, 52,* 2029-2053. https://doi.org/10.1007/s00382-018-4239-7

Funk, C., Peterson, P., Landsfeld, M., Pedreros, D., Verdin, J., Shukla, S. et al. (2015). The Climate Hazards Infrared Precipitation with Stations—A New Environmental Record for Monitoring Extremes. *Scientific Data, 2,* Article No. 150066. https://doi.org/10.1038/sdata.2015.66

Korecha, D., & Barnston, A. G. (2007). Predictability of June-September Rainfall in Ethiopia. *Monthly Weather Review, 135,* 628-650. https://doi.org/10.1175/mwr3304.1

Korecha, D., & Sorteberg, A. (2013). Validation of Operational Seasonal Rainfall Forecast in Ethiopia. *Water Resources Research, 49,* 7681-7697. https://doi.org/10.1002/2013wr013760

Kucharski, F., Parvin, A., Rodriguez-Fonseca, B., Farneti, R., Martin-Rey, M., Polo, I. et al. (2016). The Teleconnection of the Tropical Atlantic to Indo-Pacific Sea Surface Temperatures on Inter-Annual to Centennial Time Scales: A Review of Recent Findings. *Atmosphere, 7,* Article 29. https://doi.org/10.3390/atmos7020029

Manatsa, D., Chingombe, W., & Matarira, C. H. (2008). The Impact of the Positive Indian Ocean Dipole on Zimbabwe Droughts. *International Journal of Climatology, 28,* 2011-2029. https://doi.org/10.1002/joc.1695

Monerie, P., Robson, J., Dong, B., Hodson, D. L. R., & Klingaman, N. P. (2019). Effect of the Atlantic Multidecadal Variability on the Global Monsoon. *Geophysical Research Letters, 46,* 1765-1775. https://doi.org/10.1029/2018gl080903

Negash, H. T., & Waza, M. A. (2025). Diagnosis of JJAS Flood/Drought Events and the Associated Atmospheric Circulation Anomalies over Ethiopia. *Journal of Geoscience and Environment Protection, 13,* 159-185. https://doi.org/10.4236/gep.2025.134009

Nicholson, S. E. (2017). Climate and Climatic Variability of Rainfall over Eastern Africa. *Reviews of Geophysics, 55,* 590-635. https://doi.org/10.1002/2016rg000544

Segele, Z. T., & Lamb, P. J. (2005). Characterization and Variability of Kiremt Rainy Season over Ethiopia. *Meteorology and Atmospheric Physics, 89,* 153-180. https://doi.org/10.1007/s00703-005-0127-x

Seleshi, Y., & Zanke, U. (2004). Recent Changes in Rainfall and Rainy Days in Ethiopia.

International Journal of Climatology, 24, 973-983. https://doi.org/10.1002/joc.1052

Tafere, M., Olivier, J., & Jordaan, M. (2013). Climate Change Adaptation: Opportunities and Challenges from Two Communities in Ethiopia. *Journal of Environment and Earth Science, 3,* 52-67.

Tang, S., Qiao, S., Wang, B., Liu, F., Zhu, X., Feng, T. et al. (2025). Recent Changes in Enso's Impacts on the Summertime CircumGlobal Teleconnection and Mid-Latitude Extremes. *Nature Communications, 16,* Article No. 646. https://doi.org/10.1038/s41467-025-55925-8

Taye, M. T., Dyer, E., Charles, K. J., & Hirons, L. C. (2021). Potential Predictability of the Ethiopian Summer Rains: Understanding Local Variations and Their Implications for Water Management Decisions. *Science of the Total Environment, 755,* Article ID: 142604. https://doi.org/10.1016/j.scitotenv.2020.142604

Vialard, J., Jin, F., McPhaden, M. J., Fedorov, A., Cai, W., An, S. et al. (2025). The El Niño Southern Oscillation (ENSO) Recharge Oscillator Conceptual Model: Achievements and Future Prospects. *Reviews of Geophysics, 63,* e2024RG000843. https://doi.org/10.1029/2024rg000843

Waza, M. A., Zhu, W., & Teshome, A. (2025). Shifting Patterns of Ethiopian mam Rainfall: Effects of Sea Surface Temperature and Atmospheric Circulation (1981-2022). *International Journal of Climatology, 45,* e8743. https://doi.org/10.1002/joc.8743

Yang, G., Jin, Y., Zhao, Y., Di Lorenzo, E., McPhaden, M. J., & Lin, X. (2025). Improving ENSO Prediction at Longer Lead Times: Role of Off-Equatorial South Pacific Heat Content. *Geophysical Research Letters, 52,* e2024GL114540. https://doi.org/10.1029/2024gl114540

Yang, Y., An, S., Wang, B., & Park, J. H. (2020). A Global-Scale Multidecadal Variability Driven by Atlantic Multidecadal Oscillation. *National Science Review, 7,* 1190-1197. https://doi.org/10.1093/nsr/nwz216

Zhang, H., & Fan, K. (2026). K-Means Clustering Analysis of Autumn Rainfall Patterns over West China and Their Underlying Mechanisms. *Atmospheric Research, 334,* Article ID: 108745. https://doi.org/10.1016/j.atmosres.2026.108745

Zhang, R., & Delworth, T. L. (2006). Impact of Atlantic Multidecadal Oscillations on India/Sahel Rainfall and Atlantic Hurricanes. *Geophysical Research Letters, 33,* L17712. https://doi.org/10.1029/2006gl026267

Zhang, T., Jiang, X., Chen, J., Yang, S., Deng, Y., Wei, W. et al. (2021). Interannual Variability of Springtime Extreme Heat Events over the Southeastern Edge of the Tibetan Plateau: Role of a Spring-Type Circum-Global Teleconnection Pattern. *Journal of Climate, 34,* 9915-9930. https://doi.org/10.1175/jcli-d-21-0049.1